# Microstructural characteristics of cold-sprayed nanostructured WC–Co coatings

R.S. Lima[a,1], J. Karthikeyan[b], C.M. Kay[b], J. Lindemann[b], C.C. Berndt[a,*]

[a]*Department of Materials Science and Engineering, State University of New York at Stony Brook, 306 Old Engineering Building, Stony Brook, NY 11794-2275, USA*
[b]*ASB Industries, Inc., Barberton, OH 44203-1689, USA*

## Abstract

The cold-spray process was used to prepare nanostructured WC–Co coatings. The coating microstructural characteristics and phase composition were analyzed via optical microscopy, scanning electron microscopy (SEM) and X-ray diffraction (XRD). The morphology and microstructure of the nanostructured WC–Co powder were also analyzed by SEM and XRD. A 10 μm thick coating was achieved. The powder particles and coating microhardness were also evaluated and compared. The results show that there is no degradation of the WC–Co powder during the cold-spray process and well bonded and phase pure WC coating can be produced by the cold-spray process.
© 2002 Elsevier Science B.V. All rights reserved.

## 1. Introduction

### 1.1. Nanostructured materials

Nanocrystalline materials (also referred to as nanostructures, nanophase materials, or nanometer-sized crystalline solids) have crystal sizes of typically approximately 10–1000 Å (1–100 nm) in at least one dimension. Nanostructured materials come in two general morphologies: (i) nanolayered materials deposited by physical vapour deposition or electrodeposition processes and, (ii) nanograined materials, which are usually consolidated from nanostructured powders [1].

As the grain size becomes smaller, there are an increasing number of atoms associated with grain boundary sites compared to crystal lattice sites. For example, at a grain size of 100 nm, approximately 3% of all atoms are associated with grain boundaries. As the grain size is reduced to 10 nm, the percentage increases to 30; at 5 nm, approximately 50% of all atoms are associated with the grain boundary sites. The unique properties of nanograined materials are associated with the fineness of structure as well as the enhanced solubility and increasing atomic mobility associated with grain boundaries [1].

### 1.2. Cold-spray processing of nano WC–Co coatings

The cold gas-dynamic process spray method or simply cold-spray is a high-rate material deposition process in which small, unmelted powder particles (typically 1–50 μm in diameter) are accelerated to velocities on the order of 600–1000 m/s in a supersonic jet of compressed gas. Upon impact against a substrate, the solid particles deform and bond together, rapidly building up a layer of deposited material [2–5].

Cold-spray was developed in the former Soviet Union in the mid-1980s. While performing supersonic wind

*Corresponding author. Tel.: +1-631-632-8507; fax: +1-631-632-8525.

*E-mail address:* cberndt@notes.cc.sunysb.edu (C.C. Berndt).

[1] Present address: National Research Council of Canada, 75 De Mortagne Boulevard, Boucherville, Que., Canada J4B 6Y4.
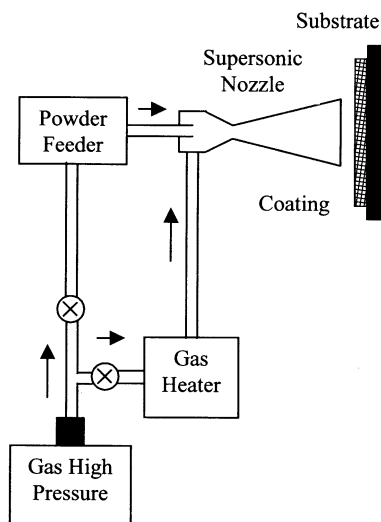
Fig. 1. Schematic of a typical cold-spray system.

tunnel tests with flows containing small tracer particles, scientists observed that above a critical particle velocity (which varies for different materials) there was a transition from particle erosion of a target surface to rapidly increasing deposition [2–4]. Based on these phenomena, a spray system was created and an US patent was issued in 1994 [6].

Fig. 1 shows the schematics of a typical cold-spray system. In cold-spray, a compressed gas, usually He, $N_2$, air or their mixtures, at inlet pressures up to 500 psi (3.4 MPa), flows through a converging–diverging nozzle to develop supersonic gas velocities. The powder particles are fed into the gas flow immediately before the converging section of the nozzle and are accelerated by the rapidly expanding gas [2–5].

The compressed gas can be introduced at room temperature, or it can be preheated in order to achieve higher gas flow velocities in the nozzle. Preheat temperatures as high as 600 °C can be used, but the gas rapidly cools as it expands in the diverging section of the nozzle. As a consequence, the dwell time of the particles in contact with hot gas is brief, and the temperatures of the solid particles at impact remain substantially below the initial gas preheat temperature [2].

The mechanisms by which the solid-state particles deform and bond to the substrate or previously deposited layers has not been well characterized. Though it has not yet been demonstrated, plastic deformation may disrupt thin surface films, such as oxides, and provide intimate conformal contact under high local pressure, allowing bonding to occur. This theory would also explain the observed minimum critical velocity necessary to achieve deposition, because sufficient kinetic energy must be available to plastically deform the solid material [2].

Calculations indicate that the particle kinetic energy at impact is typically much less than the energy required to melt the particle [2]. Micrographs of cold-sprayed coatings suggest that the deposition mechanism is primarily a solid-state process [2,3]; i.e. no material melting occurs in this process.

WC–Co coatings are well known for their use in wear resistance applications [7,8]. The hard WC particles form the major wear-resistant constituent of these materials, while the Co binder provides toughness and support [8]. Properties such as the hardness, wear resistance, and strength are influenced primarily by the WC grain size and volume fraction, and in the case of thermal spray coatings, also the porosity, the carbide and binder phase composition [8]. But due to the high temperature characteristics of the traditional thermal spray methods, such as, high velocity oxy-fuel (HVOF), plasma spray, detonation-gun, flame spray and high velocity air-fuel; the WC–Co powder tends to undergo a combination of decarburization, oxidation, reduction by reaction with the $H_2$ (plasma spray), and dissolution/reaction between the WC and Co during spraying. This behavior results in the formation of hard and brittle phases, such as, $W_2C$, W, $Co_xW_yC_z$ (crystalline and amorphous $\eta$-phases) and $WO_3$ [8–12].

Due to its low temperatures, the cold-spray process is a new alternative method for spraying not only WC–Co powders but also nanostructured materials. As an advantage, in cold-spray there is no particle melting and all the nanostructure will be kept intact during the process. In contrary, the traditional thermal spray processes require at least some partial melting of the sprayed material in order to produce adhesion/cohesion of the sprayed particles. Any melting of the nanostructured material will cause the resolidified particles to have the same microstructure as 'regular' thermal sprayed particles.

No phase transformation occurs during the cold-spray process since it is a 100% solid-state process; implying no particle melting. Therefore, oxidation, nitriding, decarburizing and any decomposition in general are avoided in this process. The as-sprayed coating phase composition should be the same as the powder phase composition.

But as it was discussed above, WC can be decomposed at temperatures lower than that of its decomposition by the reaction of the WC with the Co binder. The compositional ranges of the $\eta$-phases ($Co_xW_yC_z$) are not fixed and vary with temperature. For example, $Co_3W_3C$ exists in the range $Co_{3.1}W_{2.9}C$ to $Co_{2.2}W_{3.8}C$ from 1197 to 1427 °C [8]. These temperatures are higher than those experienced during cold-spray, where the maximum gas temperature does not exceed 600 °C [2]. The gas temperature used during this work was 540 °C.

The wettability of WC by most binder metals is better than that of the other carbides and the WC is tougher

Table 1
Spray parameters

| Main gas | $N_2$ |
|---|---|
| Main gas temperature at the gun (°C) | 540 |
| Gun pressure (psi) | 300 |
| Spray distance (mm) | 25 |

than the other carbides. The nanostructural character may improve the mechanical properties of this material. Due to its low temperatures (no WC degradation), the cold-spray process may represent a significant advancement to the spraying of nanostructured carbides.

The objective of this work is to produce nano WC–Co coatings by the cold-spray process and investigate the microstructural characteristics of cold-sprayed WC–Co coatings.

## 2. Experimental procedure

ASB Industries cold-spray system was built according to the design of its Russian inventors [6], and was used for the study reported in this article. The nanostructured WC–12%Co Metco AE7923 feedstock (Sulzer-Metco, Westbury, NY) was cold-sprayed on low carbon steel substrates. The feedstock particle size varies from 10 to 43 μm. The substrates were grit blasted with alumina just before the deposition. The typical coating thickness was 10 μm. The spray parameters applied are listed in Table 1.

The cross-section of the coating was evaluated by using an optical microscope (Nikon-Epiphot 200, Nikon Inc., Melville, NY). The coating and the cross-section of the WC–Co feedstock particles were also analyzed by scanning electron microscopy (SEM).

The Knoop microhardness measurements were performed at 10 g load for 15 s (Tukon, Instron, Canton, MA) on the coating and feedstock particle cross-sections. In order to measure the feedstock microhardness, the particles were vacuum impregnated with epoxy resin and polished. Knoop indentation was chosen because it has a shallow penetration when compared to that of Vickers. Therefore, Knoop indentation seems to be more adequate for performing microhardness measurements in small volumes, such as, powder particles.

X-ray diffraction (XRD) (Model 172a-CuKα, Philips, Almelo, Netherlands) was used to establish the phase composition of the feedstock and coating. XRD was also used to estimate the average grain size of the feedstock and coating [13–16]. The applicability of this method was confirmed by comparing results from transmission electron microscopy (TEM) and XRD techniques [15,16]. The XRD method assumes that the overall broadening of XRD peaks comprises two effects: one arising from the small coherent grain size and one arising from the atomic level microstrain; i.e. $\Delta d/d$,

where $d$ is the atomic spacing. The peak width resulting from a small grain size effect alone can be described by the Scherrer equation [13,14]:

$$B(2\theta) = \frac{K\lambda}{D\cos\theta} \qquad (1)$$

In Eq. (1), $B(2\theta)$ is the true broadening of the diffraction line measured at half maximum intensity, also known as full-width at half-maximum; $K$ is a constant (being taken as 0.9); $\lambda$ is the wavelength of the X-ray radiation; $D$ is the mean dimension of the grains and $\theta$ is the Bragg angle. Contributions due to $K\alpha_1$ and $K\alpha_2$ were deconvoluted by using the Rachinger correction [13,14], and only the $K\alpha_1$ peak widths were used for calculation. XRD of a Si specimen was used to measure the instrumental broadening, and the Cauchy correction was used to remove the instrument broadening to obtain the true crystal broadening [14]. According to Ref. [17], results from TEM and XRD of alumina feedstocks showed that the best fit was obtained when the Cauchy correction was applied to remove the instrument broadening factor. The XRD method can provide structural information regarding mean grain size along the entire sample [13–15], and the penetration distance of the X-ray beam into the sample can vary from a few to several micrometers depending on the sample characteristics.

## 3. Results and discussion

### 3.1. Feedstock morphology and phase composition

Figs. 2 and 3 show the typical feedstock particle morphology. The powder particles present the microstructural characteristics representative of agglomerated and sintered particles [8,18]. Individual nanoparticles can not be successfully thermal sprayed because of their
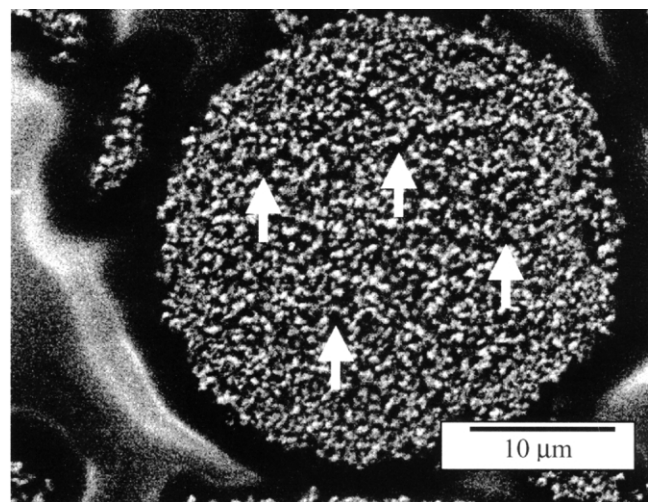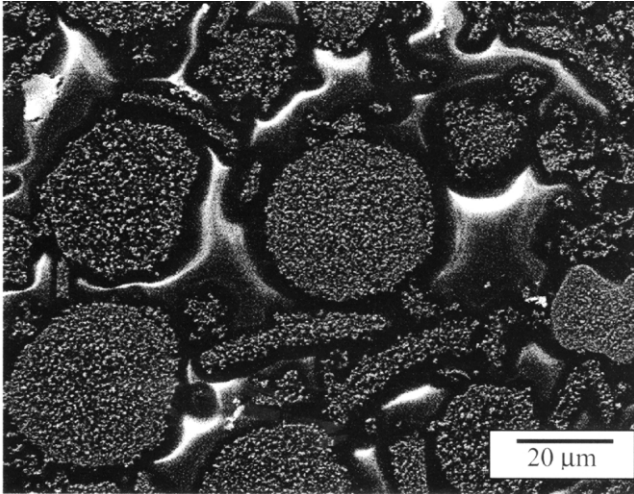


Fig. 2. Typical nanostructured WC–Co particle.

Fig. 3. General morphology of the nanostructured WC–Co particles.



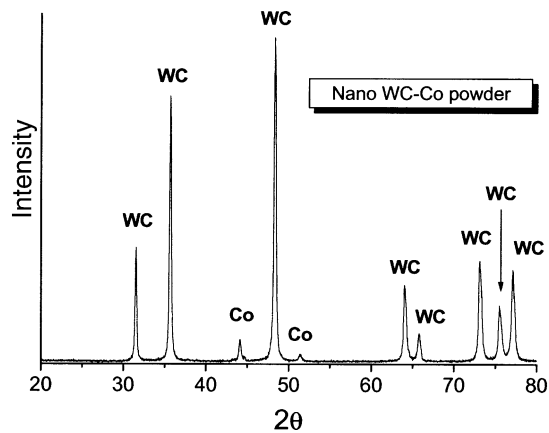Fig. 6. Cross-section of a nanostructured cold-sprayed WC–12%Co coating (SEM).



Fig. 4. XRD of the nanostructured WC–12%Co powder.

low mass [19]. Thus, they do not have the inertia required to cross the streamlines in the spray jet and would be segregated to its periphery without deposition on the substrate.
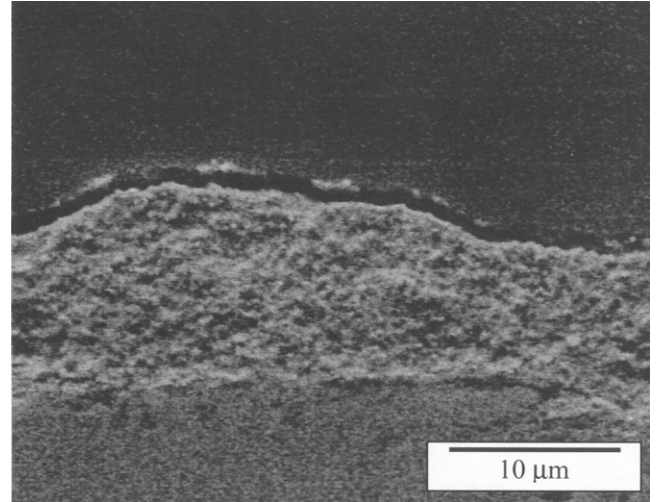
To overcome this problem, the feedstock was developed by creating an agglomeration of nanoparticles into large (micron sized) irregular shaped blocks. The agglomeration of nanoparticles into microscopic particles also allows use of existing conventional powder feeders. Each powder particle has two distinct regions. One region is light or white, representing the highly agglomerated nanoparticles of WC. The other region is dark, localized in between the microscopic particles. Some of these typical dark regions indicated in Fig. 2 are expected to be porosity presented in the agglomerated particles. Fig. 3 shows that the particles have a very irregular external morphology, changing from a sphere to a lenticular shape.

The XRD pattern of the nanostructured WC–Co powder is shown in Fig. 4. Only the presence of a well crystalline phase of WC and some amount of Co are noticed.
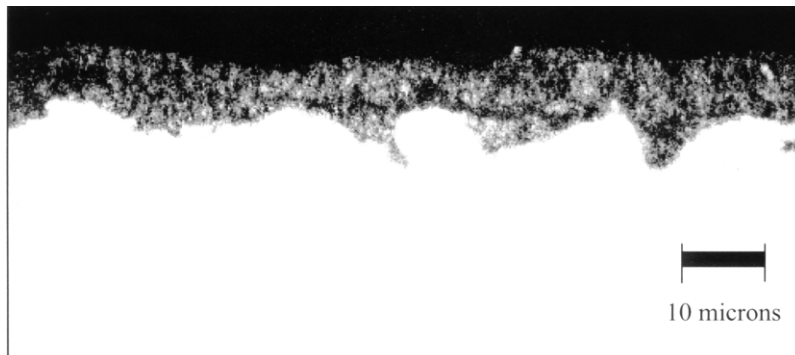


Fig. 5. Cross-section of a nanostructured cold-sprayed WC–12%Co coating (OM).
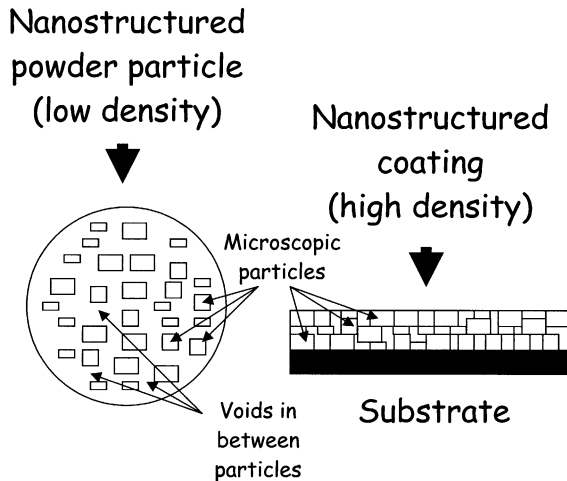
Fig. 7. Schematic of the particle densification upon impact at a high velocity.
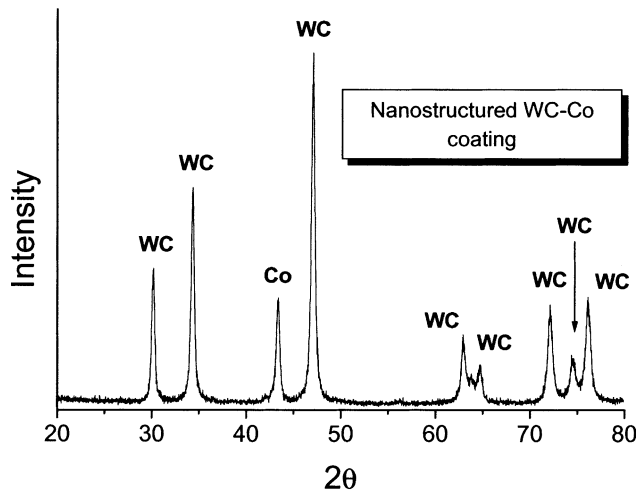


Fig. 8. XRD of the nanostructured WC–12%Co cold-sprayed coating.

### 3.2. Coating cross-section

The cross-section of the nanostructured WC–Co coating analyzed via optical microscopy (OM) and SEM are seen in Figs. 5 and 6, respectively. It is noticed that the coating is very dense, without the presence of porosity. The coating–substrate interface shows no gaps or cracks, which are characteristic feature of 'good' adhesion between the coating and the substrate.

Observing the optical micrograph, the substrate surface is very irregular, and exhibits valley and reentrant features. The coating totally fills the reentrant features and follows exactly this very irregular surface. This is probably associated with the supersonic velocities of impact presented by the cold-sprayed particles [4].

Comparing the SEM pictures of the feedstock particle and coating taken with the same magnification of $1000\times$ (Figs. 2 and 6, respectively), the irregular cross-section surface, caused by the agglomeration of microscopic particles during manufacturing is noticed. However, the structure of the powder particle is not dense when compared with the structure of the coating. It is possible to observe dark regions in the powder microstructure between adjacent microscopic particles (Fig. 2); as pointed out by arrows. Nevertheless, these dark gaps are not observed in the coating microstructure (Fig. 6); only the irregularities of the cross-section surface created by the microscopic particles are observed.

During the impact at supersonic velocities, and by the fact that the cold-spray is a solid-state process, there should be a densification of the powder particles upon impact, but not any melting. The densification will pack the microscopic particles, eliminating the voids or dark gaps between them. A schematic of the particle structure and its densification upon impact at a high velocity is shown in Fig. 7.

### 3.3. Feedstock and coating microhardness

The Knoop microhardness at 10 g load (number of measurements, $n=5$) for the nanostructured WC–12%Co powder particles is $42\pm7$ kgf/mm$^2$. However, the Knoop microhardness at 10 g load (number of measurements, $n=3$) for the nanostructured WC–12%Co cold-sprayed coating is $1225\pm282$ kgf/mm$^2$.

These experimental observations agree very well with the densification observed in the microstructures of the powder and coating and with the model described in Fig. 7, supported by the supersonic velocities of impact presented by the cold-sprayed particles [2–4].

Typical Vickers microhardness values for WC–Co coatings HVOF, D-Gun and plasma sprayed are in the range 1000–1400 kgf/mm$^2$ HV (300 g) [20,21]. At 10-g load the maximum hardness value increases considerably because the indentation impression encloses only a relatively small region of the coating. The indentation sizes are on the order of a single or few splats of the coating. This minimizes the extend of defects, such as, pores, splat boundaries and microcraking enclosed within the indentation [22]. As a consequence, the intrinsic properties of the material are preferentially measured.

However, the hardness values presented by the coating under a low load of 10 g are in the range of those presented at 300 g; considering here that Knoop and Vickers hardnesses have similar characteristics. It may be stated that the significant increase in hardness from feedstock to coating is much more an effect of particle compaction rather than nanostructural characteristics.

### 3.4. Coating phase composition

The XRD pattern of the nanostructured WC–Co coating is shown in Fig. 8. Only the presence of a

Table 2
Average grain size

| Material | Average grain size (nm) |
|---|---|
| Nanostructured feedstock WC–Co | 109 |
| Nanostructured cold-sprayed coating WC–Co | 103 |

crystalline phase of WC and some Co are noticed. None of the phases formed by the degradation of the WC–Co, normally observed in other thermal spray processes [8–12] are present in the cold-sprayed coating. The XRD patterns also agree with the fact that the deposition mechanism is primarily a solid-state process in cold-spray [2,3].

As no phase transformation is noticed, this observation also agrees with the phenomenon described in Fig. 7. The significant increase in microhardness from powder to coating ($\sim 2800\%$) can not be explained on basis of phase transformations. Sintering also can not explain the microhardness increase because of the low gas temperature and dwell time of the particles (fractions of a second) in the spray jet. The impact densification seems to be the most plausible phenomenon.

### 3.5. Feedstock and coating grain size

Table 2 shows the average grain size of the feedstock and coating. According to Ref. [13], the accuracy of a grain size determination depends mainly on the accuracy with which the pure diffraction breadth $\beta$ can be measured. In Ref. [13] curves of pure diffraction breadth/sample breadth ($\beta/B$) versus instrument broadening/sample breadth ($b/B$) are observed. According to Ref. [13], as the grain size becomes very large (and $\beta$ very small), the ratio $b/B$ inevitably increases into the unfavorable range above 0.50, and the ratio $\beta/B$ decreases in spite of the best possible adjustment of the experimental conditions. As a consequence, one must choose the regions where the high values of $\beta$ (or $\beta/B$) are found. Thus, based on the above statement, the regions where the ratio $b/B$ is below 0.50 should be chosen by the observer. For the samples and experimental conditions found in this work, the peak (1 0 1) of the WC (100%) at $2\theta \sim 48°$ presented optimal characteristics for analysis.

The Scherrer equation was deduced under the assumption that only a small grain size is responsible for peak broadening [13–15]. Strain effects, which may influence the peak broadening are not taken into account [13–15]. In thermal spray, the occurrence of residual stress effects is known [7,23]. However, the residual stresses are normally associated to high temperatures involved in the spray process [7,23]. Since the cold-spray process temperatures much lower than that of the melting point

of the sprayed materials, then the residual stress effects from thermal origin should then be minimized.

In fact, when comparing the results of Table 2, it is noticed that the average grain size of the feedstock particles and the coating are quite similar. This observation collaborates with the issues of the above discussion about residual stress from thermal origin.

However, compressive stresses resulting from the impact of high velocity particles against the substrate surface might be present. As discussed in other section, the impact produces a densification in the WC–Co particles. This densification effect might exhibit similar characteristics to those of 'shot-peening'; i.e. compressive stresses. Nonetheless, if compressive residual stresses are present, they do not seem to be making a significant effect on average grain size measured by XRD technique (Table 2).

### 4. Conclusions

The nanostructured WC–Co cold-sprayed coating has a high density and microhardness when compared to those of the nanostructured feedstock. The coating microhardness enhancement is much more dependent on the impact velocity than the nanostructured particle microhardness itself. The impact of the particles against the substrate at supersonic velocities, promotes a densification in each nanostructured particle. There is no significant difference between the average grain size of the nanostructured feedstock and coating. It is possible to produce pure and well bonded nanostructured WC–Co coatings via cold-spray processing.

### Acknowledgments

### References

[1] M. Gell, JOM October (1994) 30.
[2] R.C. Dykhuizen, M.F. Smith, J. Therm. Spray Tech. 7 (2) (1998) 205.
[3] R.C. McCune, A.N. Papyrin, J.N. Hall, W.L. Riggs, P.H. Zajchowski, in: C.C. Berndt, S.S. Sampath (Eds.), Advances in Thermal Spray Science and Technology, ASM International, Materials Park, OH, 1995, p. 1.
[4] D.L. Gilmore, R.C. Dykhuizen, R.A. Neiser, T.J. Roemer, M.F. Smith, J. Therm. Spray Tech. 8 (4) (1999) 576.
[5] J. Karthikeyan, C.M. Kay, J. Lindeman, R.S. Lima, C.C. Berndt, in: C.C. Berndt (Ed.), Thermal Spray: Surface Engineering via Applied Research, ASM International, Materials Park, OH, 2000, p. 255.
[6] A.P. Alkhimov, A.N. Papyrin, V.F. Kosarev, N.I. Nesterovich, M.M. Shuspanov, U.S. Patent No. 5,302,414, April, 1994.
[7] L. Pawlowski, The Science and Engineering of Thermal Spray Coatings, Wiley, Chichester, England, 1995.

[8] H.L. de Villiers Lovelock, J. Therm. Spray Tech. 7 (3) (1998) 357.

[9] H.L. de Villiers Lovelock, P.W. Richter, J.M. Benson, P.M. Young, J. Therm. Spray Tech. 7 (1) (1998) 97.

[10] J.R. Fincke, W.D. Swanck, D.C. Haggard, in: C.C. Berndt, S.S. Sampath (Eds.), Thermal Spray Industrial Applications, ASM International, Materials Park, OH, USA, 1994, p. 325.

[11] K. Korpiola, P. Vuoristo, in: C.C. Berndt (Ed.), Thermal Spray: Practical Solutions for Engineering Problems, ASM International, Materials Park, OH, 1996, p. 177.

[12] C.J. Li, A. Ohmori, Y. Harada, J. Therm. Spray Tech. 5 (1) (1996) 69.

[13] H.P. Klug, L.E. Alexander, X-Ray Diffraction Procedures, second ed., Wiley, NY, USA, 1974.

[14] B.E. Warren, X-Ray Diffraction, Dover Publications, Inc, NY, USA, 1990.

[15] H.G. Jiang, M. Ruhle, E.J. Lavernia, J. Mater. Res. 14 (2) (1999) 549.

[16] T. Chraska, Ph.D. Thesis, State University of New York at Stony Brook, NY, USA, 1999.

[17] T. Ekstron, C. Chatfield, W. Wruss, M. Maly-Schreiber, J. Mater. Sci. 20 (1985) 1266.

[18] H.L. de Villiers-Lovelock, S. Luyckx, in: C.C. Berndt (Ed.), Surface Engineering via Applied Research, ASM International, Materials Park, OH, 2000, p. 647.

[19] S. Eidelman, X. Yang, NanoStructured Mater. 9 (1997) 79.

[20] R. Schwetzke, H. Kreye, J. Therm. Spray Tech. 8 (3) (1999) 433.

[21] R.C. Tucker, J. Vac. Sci. Tech. 11 (4) (1974) 725.

[22] J.P. Singh, M. Sutaria, M. Ferber, Ceramic Eng. Sci. Proc. 18 (4b) (1997) 191.

[23] S. Kuroda, T. Fukushima, S. Kitahara, Thin Solid Films 164 (1988) 157.